Journal of Asian Concrete Federation

journal homepage: https://jacf.sfulib3.publicknowledgeproject.org/index.php/jacf

Limit State Analysis of Pre-stressed Self-Lifting Octagonal Reinforced High-Strength Concrete Wind Towers with a Hub Height of 200 m

Chao Shen[1], Rongjun Yang[2], Ziteng Wang[1,3], Junqiang Wen[2], Shuo Zhang[2], Yuncheng Ge[2], Hanyuanbin Wang[3], Xiangguo Wu[4,5*], Arun Paudel[6*]

[1] *School of Civil Engineering, Harbin Institute of Technology, Harbin, 150001, China.*
[2] *BCEG Advanced Construction Materials Co., Ltd., Beijing, 100055, China.*
[3] *Wuhan University of Science and Technology, Wuhan, 430081, China.*
[4] *College of Civil Engineering, Fuzhou University, Fuzhou, 350108, China.*
[5] *Key Lab of Structures Dynamic Behavior and Control of the Ministry of Education, Key Lab of Smart Prevention and Mitigation of Civil Engineering Disasters of the Ministry of the Industry and Information Technology, Harbin Institute of Technology, Harbin, 150090, China.*
[6] *Pulchowk Campus, Institute of Engineering, Tribhuvan University, Kathmandu, Nepal.*

A B S T R A C T

This paper presents a 200-meter pre-stressed self-lifting steel–concrete composite tower designed for multi-megawatt wind turbines with ultra-high hub heights, detailing its structural concept, design parameters, and performance analysis. Using the ABAQUS finite element software, the static performance of the tower was analyzed and checked against IEC 61400-6 (2020) and other relevant national codes, and the stresses in towers with internal and external pre-stressing were compared. The results show that the tower has good mechanical performance. The arrangement of internal and external pre-stressing tendons has little influence on the lateral displacement of the tower. Under the S_1 condition, the principal compressive stress of the externally pre-stressed tower along the section height is slightly larger than that of the internally pre-stressed tower. Under the S_2 condition, the principal tensile stress of the externally pre-stressed tower along the section height is slightly smaller than that of the internally pre-stressed tower. Similarly, under the S_3 working condition, the maximum vertical stress along the height of the externally pre-stressed tower is slightly smaller than that of the internally pre-stressed tower. Apart from small local tensile stresses, the rest of the tower satisfies the full-section compression requirement.

Keywords: Wind power generation; Conceptual design; Self-lifting tower; External pre-stressing; Internal pre-stressing

1. Introduction

The rapid growth of global energy consumption and the urgent need for sustainable alternatives have drawn increasing attention to renewable sources. Among these, wind energy has become a particularly important and widely utilized resource. Wind turbine systems are characterized by tall, top-heavy structures composed of several load-bearing components, including the foundation, tower body, flanges, nacelle, and blades. The tower, in particular, plays a crucial role in providing overall strength, stiffness, and stability. Most existing towers worldwide range from several tens of meters to just above 100 m, and large-scale wind power towers commonly exceed 100 m (Wang et al., 2019). Steel towers remain the most extensively studied and applied form. Although research has increasingly considered steel–concrete composite configurations, their heights have so far been limited to less than 170 m. With the continuous increase in turbine power ratings, the demand for even taller towers will inevitably intensify. This trend highlights the importance of investigating super-high composite tower forms that can overcome both structural and construction challenges.

When designing ultra-high towers, the selection of a rational tower form is essential to ensure reliable structural performance. Under the combined effects of aerodynamic forces and blade rotation, stress distribution and load-bearing behavior become critical design concerns (Shan, 2009). Conventional cone-shaped composite towers currently

* Corresponding author: wuxiangguo@hit.edu.cn; arun.paudel@pcampus.edu.np

DOI http://dx.doi.org/10.18702/acf.2026.12.1.???

Received: 24-Jun-2026; Revised: 19-Aug-2026; Accepted: 03-Sep-2026; Published online: 17-November-2026

ISSN 2465-7964, eISSN 2465-7972. Copyright © Asian Concrete Federation, All rights reserved.

Proof Reading

used in practice face difficulties as their height increases, because lifting operations become increasingly constrained by the capacity of available tower cranes. To address this, new structural concepts are needed. One promising approach is the introduction of self-lifting technology, which connects two sections of the concrete tower through intermediate corbels, thereby enabling the tower to lift itself and reducing dependence on heavy lifting equipment. Compared with multi-stage lifting, a single self-lifting operation shortens construction time, simplifies procedures, and reduces risks. In addition, adopting an octagonal, fully assembled plate-unit configuration further improves efficiency by enabling modular assembly and significantly reducing mold fabrication costs.

Extensive research has been carried out worldwide on the static performance of wind turbine towers. For instance, Song and Chen (2012) analyzed the static performance of a 2.5 MW pre-stressed concrete tower, identifying weak points and calculating internal forces at critical sections. Zhang (2015) investigated a 5 MW octagonal pre-stressed concrete tower under multiple load cases and validated results against experimental data. Dong (2015) and Liu (2016) examined hollow sandwich steel tube–concrete towers and splicing methods through axial compression tests, revealing failure modes under static loads. Gu (2009) modeled a 97.7 m hybrid tower and found that performance improved when the concrete section accounted for one-third of the total height. Vernardos et al. (2021) proposed a steel–grouted–steel sandwich segment, showing enhanced capacity, stiffness, and stability without increasing steel usage. Other contributions include Bazeos and Hatzigeorgiou (2002), who used finite element methods to assess load combinations that induce buckling; de Lana et al. (2021), who applied genetic algorithms to optimize a 100 m pre-stressed concrete tower; Brughuis (2003), who compared steel and composite towers, highlighting the latter's economic advantages; and Ma et al. (2014), who demonstrated the benefits of prefabricated post-tensioned reactive powder concrete towers. While these studies have advanced understanding of tower performance, they largely focus on traditional cone-shaped or circular-section towers. Such forms face clear height limitations, cannot be modularized as readily as polygonal towers, and generally emphasize incremental optimization rather than conceptual innovation.

To address these limitations, this study proposes and evaluates a 200 m pre-stressed steel–concrete composite self-lifting tower with an octagonal plate-unit assembly. The paper introduces the tower's conceptual design, design parameters, and structural configuration. Static performance is investigated using ABAQUS finite element simulations, and compliance is verified against IEC 61400-6 (2020) and relevant national codes. Performance checks include lateral displacement under S_1 loading, compressive stress distribution under S_1, crack resistance under S_2, and decompression under S_3. In addition, internal and external pre-stressing arrangements are compared to assess their influence on structural behavior. The results demonstrate that the proposed tower exhibits favorable mechanical performance, with minimal differences between internal and external pre-stressing layouts. This research provides both a novel structural concept and performance evidence, offering a practical reference for the engineering design and application of next-generation super-high wind turbine towers.

2.Tower design parameters

2.1 Structure overview

Figures 1a and 1b show the elevation and plan view of the tower, respectively. The relevant parameters of the tower are as follows: T_1 denotes the bottom concrete tower cylinder, T_2 the concrete tower cylinder bracket segment, T_3 the middle concrete tower cylinder, and T_4 the top steel tower cylinder. The corresponding dimensions are defined as: H_1 – height of the bottom concrete tower cylinder, H_2 – height of the bracket segment, H_3 – height of the middle concrete tower cylinder, and H_4 – height of the top steel tower cylinder. The diameters are represented as D_1 (bottom concrete tower cylinder), D_2 (middle concrete tower cylinder), D_3 (bottom end of the top steel tower cylinder), and D_4 (top of the top steel tower cylinder). The wall thicknesses are given as t_1 (bottom concrete tower body), t_2 (middle concrete tower body), t_3 (bottom end of the top steel tower body), and t_4 (top of the top steel tower body). Similarly, h_1 and h_2 denote the thicknesses of the bracket segments of the bottom and middle concrete tower cylinders, respectively, while h_3 represents the height of the prefabricated transition segment. The bracket segment widths are denoted as l_1 (bottom concrete tower cylinder) and l_2 (middle concrete tower cylinder). Finally, b_1 and b_2 indicate the widths of the inner and outer plates of the bottom concrete tower cylinder, while b_3 and b_4 represent the widths of the inner and outer plates of the middle concrete tower cylinder.

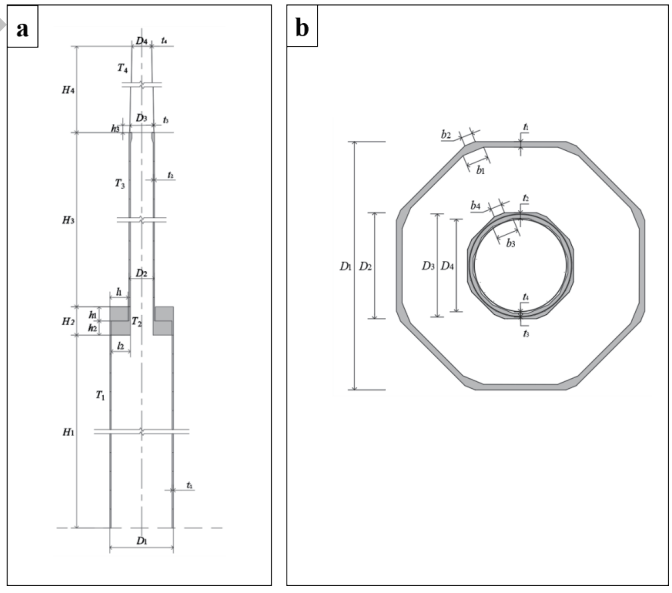


Figure 1. (a) Elevation section of tower and (b) plan view of tower

The structure consists of a slab-assembled, self-lifting tower cylinder, in which the concrete tower section is constructed

Proof Reading

from prefabricated slabs. The self-lifting technology enables the middle concrete tower cylinder and the top steel tower cylinder to lift themselves through the use of self-lifting corbels. Each concrete segment is composed of eight standard prefabricated wall panels, which are cast in simple molds that significantly reduce mold production costs. Only six types of wall panel molds are required for the entire concrete tower, allowing rapid and large-scale fabrication of prefabricated components. The tower employs a single self-lifting operation, which effectively shortens construction and hoisting time and minimizes the need for large tower cranes. The bracket segment is equipped with self-lifting holes, which are sealed and connected with high-strength anchor bolts after the lifting device is removed, thus achieving a dry connection. Overall, the construction process is straightforward. Furthermore, to satisfy the clearance requirements between the blades and the tower body, a two-stage tower system has been adopted, which effectively resolves the clearance issue.

2.2 Tower material considerations

The tower is mainly made of concrete and steel. C_{60}–C_{100} concrete can be used for the concrete tower section, HRB_{400}–HRB_{500} reinforcement can be used for the ordinary reinforcement, 15.2 mm steel strand can be used for the pre-stressed reinforcement, and Q_{345} steel can be used for the steel cylinder section. In the preliminary design, C80 concrete was used for the tower cylinder, HRB_{400} reinforcement for the ordinary reinforcement, 15.2 mm steel strand for the pre-stressed reinforcement, and Q_{345} steel for the steel cylinder section. The specific material properties are listed in Table 1.

Table 1. Mechanical parameters of materials

Material	Elastic modulus (N/mm^2)	Poisson's ratio	Density (kg/m^3)	Yield strength (MPa)	Material properties	Remarks
C_{80}	38000	0.2	2400	/	Elastoplasticity	/
Rebar (HRB_{400})	200000	0.3	7850	360	Elasticity	/
Steels (Q_{345})	200000	0.3	7850	335	Elasticity	$16 < t \leqslant 40$
				305	Elasticity	$80 < t \leqslant 100$

Table 2. Material parameters of pre-stressed reinforcement

Type	Nominal diameter (mm)	Standard value of ultimate strength f_{ptk} (N/mm^2)	Design value of tensile strength f_{py} (N/mm^2)	Design value of compressive strength f'_{py} (N/mm^2)	Elastic modulus E_s (N/mm^2)
Steel strand	15.2	1860	1320	390	1.95×105

3.Performance analysis of typical tower cylinder

3.1 Basic parameters of typical tower cylinder

The hub height of the tower is 200 m. The concrete tower section is octagonal, with a circumscribed diameter of 13.5 m at the tower bottom and a plate thickness of 300 mm; the total height of the bottom concrete tower section is 90 m. The middle concrete tower section is also octagonal. To ensure sufficient clearance for the rotor blades, the circumscribed-circle diameter at the bottom of the T3 section is 5.4 m, the plate thickness is 300 mm, and the height is about 76 m. The prefabricated transition section and the steel tower section are set on top of T3. The transition section is about 1.5 m high. The steel tower section (T_4) is 30 m high and has a variable wall thickness, tapering from 40 mm at the bottom to 22 mm at the top. In this paper, a 4.5 MW wind turbine is considered. The typical tower cylinder dimensions are given in Table 3, and the nacelle and rotor parameters are given in Table 4.

Proof Reading

Table 3. Basic parameters of the typical tower

Parameter symbol	Dimensions (mm)	Parameter symbol	Dimensions (mm)
H_1	84000	t_4	22
H_2	6000	h_1	3000
H_3	76000	h_2	3000
H_4	30000	h_3	1500
D_1	13500	l_1	3935
D_2	5400	l_2	4050
D_3	5040	b_1	1200
D_4	4220	b_2	600
t_1	300	b_3	1200
t_2	300	b_4	600
t_3	40	/	/

Table 4. Fan parameters

Component name	Coordinate axis	x	y	z
Rotor	Position (m)	5.295	0	2.25
	Mass (kg)		105305	
Nacelle	Position (m)	0.08	0.132	1.853
	Mass (kg)		133000	

3.2 Finite element model

ABAQUS is a powerful engineering simulation software package consisting of the Standard and Explicit solvers, ABAQUS/CAE, and other specialized modules (Gudayu et al., 2022). It has excellent analysis capability and is applicable to almost all static and dynamic problems. It also provides extensive element and material-model libraries and can simulate a wide variety of complex engineering problems (Barbero, 2023). Therefore, ABAQUS was used for the finite element simulations in this paper (Shi and Zhang, 2021). This paper mainly analyzes the static performance of two pre-stressed models, one with internal and one with external pre-stressing, using the typical tower cylinder dimensions given in Table 3; the two models are described in Table 5.

In the finite element model, the concrete tower and the steel tower are modeled using C3D8R solid elements, while conventional reinforcement bars and pre-stressed tendons are modeled using T3D2 truss elements. The overall mesh size is approximately 200 mm, with local refinement to approximately 50 mm in the door openings, supports, anchorage zones, and transition sections. An Embedded constraint is applied between the reinforcement bars and the concrete, while a Tie constraint is applied between the external pre-stressed tendons and the deviator blocks. The base of the tower is treated as a fixed boundary. Comparative analyses across three mesh densities show that the differences in key displacement and stress results are less than 3%, satisfying the mesh convergence criteria. The present serviceability analysis is conducted using a linear elastic material model for all components.

4. Application of load

In ABAQUS, pre-stressing is mainly applied by either the initial strain method or the cooling method. In this paper, the cooling method was used. In this method, an expansion coefficient is assigned to the pre-stressing tendon and its temperature is then reduced, so that the tendon shrinks and the pre-stress is induced (Zhou et al., 2015).

The layout of the pre-stressed tendons is shown in Figure 2a. In the T_1 section, 6 tendons are arranged in each slab unit, giving a total of 48 tendons. In the T_3 section, 5 tendons are arranged in each slab unit, giving a total of 40 tendons. Ten steel strands are placed in each duct. Because the pre-stress loss differs between sections when the tendons are tensioned, the effective pre-stress also differs. Therefore, in this model the tendons are divided into segments according to the elevation of each tower section, so that the effective pre-stress, and hence the cooling temperature, of each elevation segment can be obtained. The segmentation of the tendons is shown in Figures 2b and 2c.

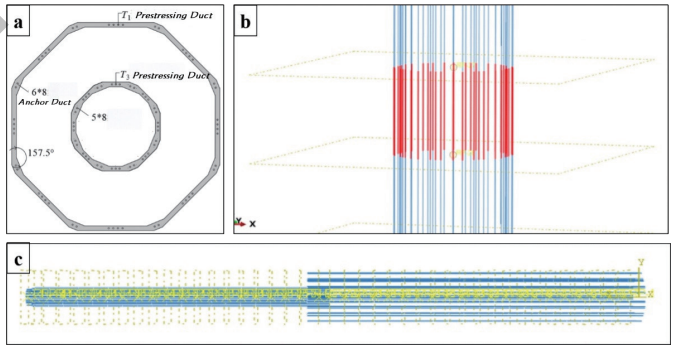


Figure 2. (a) Layout of pre-stressed reinforcement, (b) details of pre-stressed reinforcement cutting, and (c) segmentation of pre-stressed reinforcement

In the cooling method, the pre-stress loss in each part of the tendon is first calculated, the effective pre-stress is then determined, and finally the cooling temperature of the tendon is computed. The pre-stress losses were calculated in accordance with Section 10.2 of the Code for Design of Concrete Structures (GB 50010, 2010), and the cooling temperature was calculated as follows:

Proof Reading

Table 5. Internal and external pre-stressing models

Model number	Pre-stressing category	Number of tendons	Nominal diameter of steel strand (mm)	Concrete grade	Ordinary reinforcement grade	Steel grade
IP-C_{80}	Internal	48/40	15.2	C_{80}	HRB400	Q_{345}
EP-C_{80}	External	48/40	15.2	C_{80}	HRB400	Q_{345}

Temperature calculation:

$$\sigma_{p0}=N_{p0}/A_p \quad (1)$$

$$\varepsilon_{th}=\sigma_{p0}/_{Ep} \quad (2)$$

$$\varepsilon_{th}=\alpha\Delta t \quad (3)$$

$$\Delta t=\frac{N_{p0}}{\alpha E_p A_p} \quad (4)$$

Where,

σ_{p0} ——Initial tensile stress of pre-stressed tendons;

N_{p0} ——Initial tensile force of pre-stressed tendons;

A_p ——Cross-sectional area of pre-stressed tendons;

ε_{th} ——Equivalent thermal strain of pre-stressed tendons;

E_p ——Elastic modulus of pre-stressed tendons;

α ——Linear expansion coefficient of pre-stressed tendons;

Δt ——Temperature drop of pre-stressed tendons.

The final cooling temperature of the pre-stressed tendons in each segment is the average of the temperatures at its upper and lower ends. The pre-stress losses and the resulting cooling temperatures of the tendons in each segment are listed in Table 6.

After the pre-stress was applied, the external loads were applied. The external loads were applied at the center of each level by means of a horizontal shear force, bending moment, torque, and gravity load. The specific application process is shown in Figure 3.

5.Finite element analysis results of the internally pre-stressed tower cylinder (IP-C_{80})

The finite element simulations in this paper follow the specification of IEC 61400-6 (2020). The relevant calculations were carried out for the tower cylinder under the serviceability limit state, which is reached when the structure or a component attains a specified limit value for normal use or a specified state for durability.

According to the IEC 61400-6 (2020) specification, three load levels are defined for wind turbine structures. The first, S_1, represents the load characteristic value level under normal and transportation conditions, corresponding to the extreme values of all design conditions. The second, S_2, refers to a frequent load level with a probability of exceedance of 0.01% under the design load case (DLC) 1.1. The third, S_3, indicates a frequent load level with a 1% probability of exceedance under DLC 1.1. Here, DLC 1.1 refers to the design load case in which the wind turbine generator system operates under normal power production with the normal turbulence model, within the wind speed range of $V_{in}<V_{hub}<V_{out}$.

According to the requirements of the specification, the lateral displacement and stress of the tower cylinder under S_1 working condition shall be checked, the tower cylinder under S_2 working condition shall be checked for crack resistance, and the tower cylinder under S_3 working condition shall be checked for decompression.

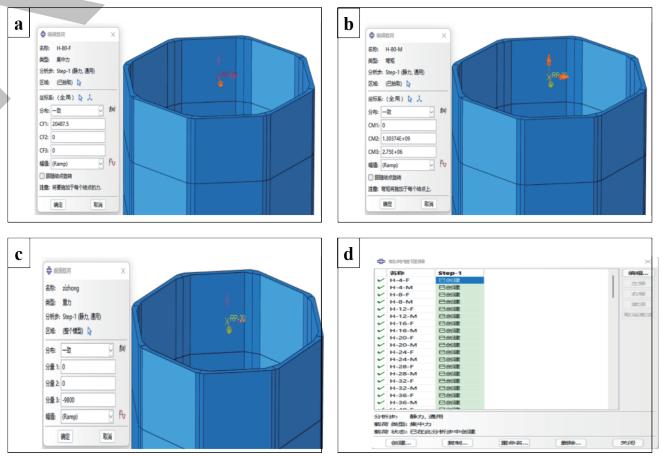


Figure 3. (a) Application of horizontal shear force, (b) application of bending moment and torque, (c) application of gravity, (d) load application manager

5.1 Checking calculation of tower top lateral displacement under S_1 working condition

According to IEC 61400-6 (2020), under S_1 level, the limit value of horizontal displacement angle shall comply with the relevant provisions of the current national standard GB

Proof Reading

Table 6. Prestressing loss and cooling temperatures of the tendons

Tower segment	level	σ_{l1} /MPa	σ_{l2} /MPa	σ_{l4} /MPa	σ_{l5} /MPa	σ_{p0} /MPa	Δt / °C	Cooling temperature / °C
/	0	9.45	52.87	48.83	58.63	1229.27	504.31	/
M01	4	9.45	61.24	48.83	58.51	1220.99	500.92	502.62
M02	8	9.45	69.61	48.83	58.40	1212.71	497.52	499.22
M03	12	9.45	77.98	48.83	58.28	1204.43	494.12	495.82
M04	16	9.45	86.35	48.83	58.16	1196.15	490.73	492.43
M05	20	9.45	94.72	48.83	58.04	1187.87	487.33	489.03
M06	24	9.45	103.09	48.83	57.92	1179.59	483.93	485.63
M07	28	9.45	111.46	48.83	57.81	1171.31	480.54	482.24
M08	32	9.45	119.83	48.83	57.69	1163.03	477.14	478.84
M09	36	9.45	128.20	48.83	57.57	1154.75	473.74	475.44
M10	40	9.45	136.57	48.83	57.45	1146.47	470.35	472.05
M11	44	9.45	144.94	48.83	57.34	1138.19	466.95	468.65
M12	48	9.45	153.31	48.83	57.22	1129.91	463.55	465.25
M13	52	9.45	161.68	48.83	57.10	1121.63	460.16	461.86
M14	56	9.45	170.05	48.83	56.98	1113.35	456.76	458.46
M15	60	9.45	178.42	48.83	56.87	1105.07	453.36	455.06
M16	64	9.45	186.79	48.83	56.75	1096.80	449.97	451.67
M17	68	9.45	195.16	48.83	56.63	1088.52	446.57	448.27
M18	72	9.45	203.53	48.83	56.51	1080.24	443.17	444.87
M19	76	9.45	211.90	48.83	56.39	1071.96	439.78	441.48
M20	80	9.45	220.27	48.83	56.28	1063.68	436.38	438.08
M21	84	9.45	228.64	48.83	56.16	1055.40	432.98	434.68

Proof Reading

Tower segment	level	σ_{l1} /MPa	σ_{l2} /MPa	σ_{l4} /MPa	σ_{l5} /MPa	σ_{p0} /MPa	Δt / °C	Cooling temperature / °C
M22	90	9.45	241.20	48.83	55.98	1042.98	427.89	430.44
/	84	9.45	52.87	48.83	74.94	1217.58	499.52	/
M23	92	9.45	69.61	48.83	74.46	1201.20	492.80	496.16
M24	96	9.45	77.98	48.83	74.22	1193.01	489.44	491.12
M25	100	9.45	86.35	48.83	73.98	1184.82	486.08	487.76
M26	104	9.45	94.72	48.83	73.74	1176.63	482.72	484.40
M27	108	9.45	103.09	48.83	73.50	1168.45	479.36	481.04
M28	112	9.45	111.46	48.83	73.26	1160.26	476.00	477.68
M29	116	9.45	119.83	48.83	73.02	1152.07	472.64	474.32
M30	120	9.45	128.20	48.83	72.78	1143.88	469.28	470.96
M31	124	9.45	136.57	48.83	72.54	1135.69	465.93	467.61
M32	128	9.45	144.94	48.83	72.30	1127.51	462.57	464.25
M33	132	9.45	153.31	48.83	72.06	1119.32	459.21	460.89
M34	136	9.45	161.68	48.83	71.82	1111.13	455.85	457.53
M35	140	9.45	170.05	48.83	71.58	1102.94	452.49	454.17
M36	144	9.45	178.42	48.83	71.34	1094.75	449.13	450.81
M37	148	9.45	186.79	48.83	71.10	1086.56	445.77	447.45
M38	152	9.45	195.16	48.83	70.86	1078.38	442.41	444.09
M39	156	9.45	203.53	48.83	70.62	1070.19	439.05	440.73
M40	160	9.45	211.90	48.83	70.38	1062.00	435.69	437.37
M41	166	9.45	224.46	48.83	70.02	1049.72	430.65	433.17

Proof Reading

50135 (2019). Referring to the Design Standard for High-rise Structures, the horizontal displacement at any point under the characteristic value of wind load and other loads shall not exceed 1/100 of the height of that point above the ground. Under S_1 working condition, the maximum horizontal displacement at the top of the wind turbine tower cylinder is 868.9 mm, which is less than the allowable displacement of 1975 mm (L/100). The displacement of the wind turbine tower cylinder under load meets the specification requirements, as shown in Figure 4.

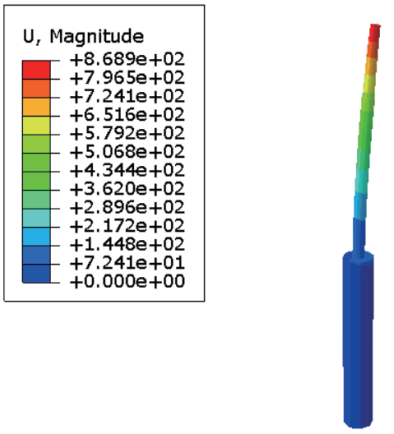


Figure 4. Contour plot of tower displacement

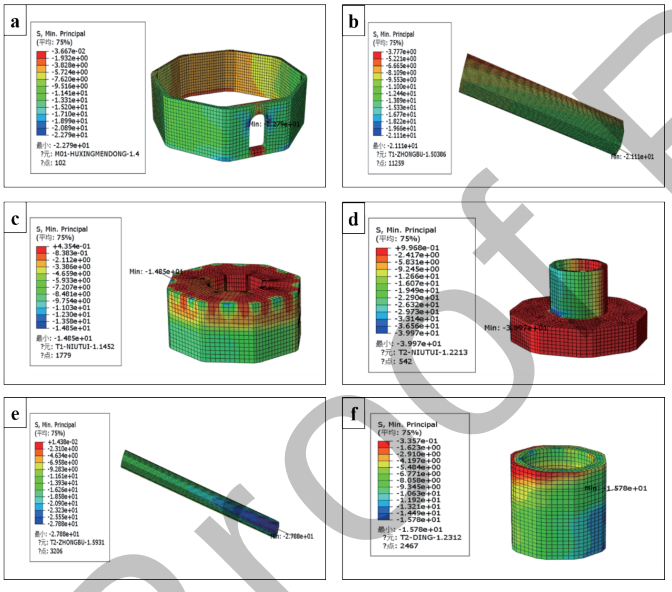


Figure 5. Contour plot of principal compressive stress of concrete tower cylinder: (a) M01 door opening segment (Min Principal: 22.79 MPa), (b) M02–M21 segment (Min Principal: 21.11 MPa), (c) M22 bracket segment (Min Principal: 14.85 MPa), (d) M23 bracket segment (Min Principal: 39.97 MPa), (e) M24–M40 segment (Min Principal: 27.88 MPa), (f) M41 segment (Min Principal: 15.78 MPa)

5.2 Checking calculation of principal compressive stress under S_1 working condition

According to IEC 61400-6 (2020) specification, under S_1 level, the maximum compressive stress limit in concrete is $0.6f_{ck}$, where f_{ck} is the characteristic compressive strength of concrete cylinder specimens. Xin (2015) showed that the strength ratio of the standard cylinder specimen to the standard cube specimen is approximately 0.8. Therefore, the maximum compressive stress limit for C_{80} concrete is $0.6 \times 0.8 \times 80 = 38.4$ MPa. At S_1 level, the tensile stress in ordinary reinforcement shall not exceed $0.9f_{yk}$, that is, for HRB_{400} reinforcement, the tensile stress shall not exceed $0.9 \times 400 = 360$ MPa. The stress of pre-stressed reinforcement (after short-term loss) shall not exceed $0.75f_{pk}$. For the 1860 grade steel strand of this structure, it is limited to $0.75 \times 1860 = 1395$ MPa.

1.Stress checking calculation of concrete tower cylinder

According to IEC 61400-6 (2020) specification, under S_1 level, the maximum compressive stress limit of C80 concrete is 38.4 MPa. Except for the M23 bracket segment, all other concrete segments meet the requirements of the specification (Figure 5). Because of the variable cross-section of the M23 bracket segment, stress concentration occurs at the abrupt change of stiffness where the cross-section changes suddenly. The peak stress at this location is 39.97 MPa, which is slightly higher (by about 4%) than the limit value required by the specification. To mitigate the effect of stress concentration in this region, local structural modifications such as introducing a smoother variable cross-section or localized thickening could be adopted.

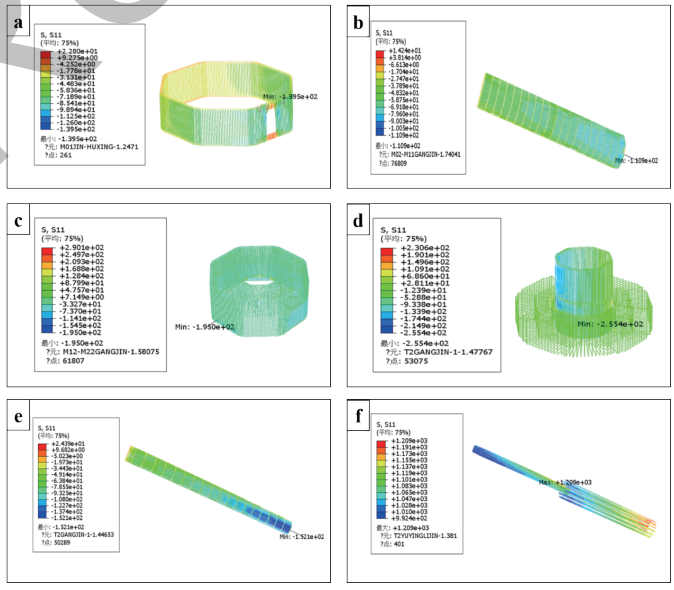


Figure 6. Stress contour plot of concrete tower cylinder reinforcement: (a) M01 door opening segmental reinforcement (S11 Max: 139.5 MPa), (b) M02–M21 section reinforcement (S11 Max: 110.9 MPa), (c) M22 bracket segment reinforcement (S11 Max: 195.0 MPa), (d) M23 bracket segment reinforcement (S11 Max: 255.4 MPa), (e) M24–M41 section reinforcement (S11 Max: 152.1 MPa), and (f) Pre-stressed reinforcement (S11 Max: 1209.0 MPa)

Proof Reading

2.Reinforcement checking calculation of concrete tower

According to IEC 61400-6 (2020), under S_1 level, the tensile stress in ordinary reinforcement shall not exceed 360 MPa, and the stress of pre-stressed reinforcement (after short-term loss) shall not exceed 1395 MPa. The stresses in both the ordinary and the pre-stressed reinforcement of the structure meet the requirements (Figure 6).

5.3 Crack resistance checking calculation under S_2 working condition

According to IEC 61400-6 (2020), under S_2 level, the maximum tensile stress in concrete shall not exceed the characteristic value of the tensile strength of concrete. For C80 concrete, the characteristic tensile strength of concrete is 3.11 MPa. Figure 7 shows the principal tensile stress contour plot of concrete tower under S_2 level.

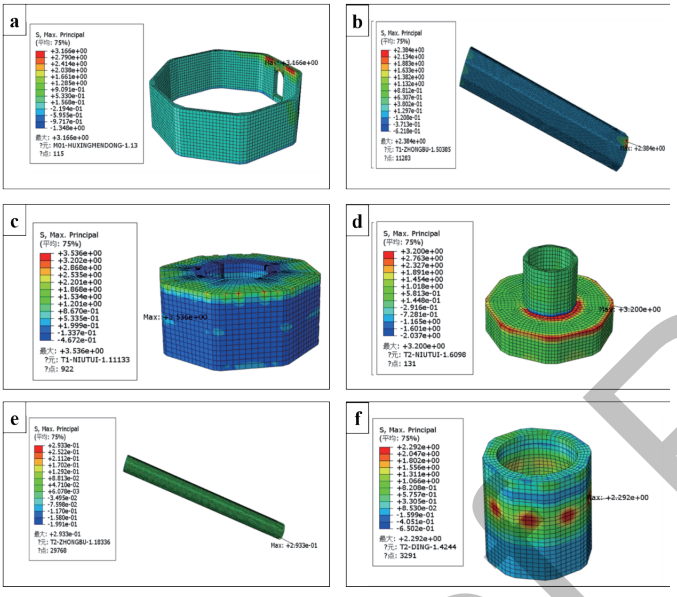


Figure 7. Contour plot of principal tensile stress of concrete tower cylinder: (a) M01 door opening segment (Max Principal: 3.16 MPa), (b) M02–M21 segment (Max Principal: 2.38 MPa), (c) M22 bracket segment (Max Principal: 3.54 MPa), (d) M23 bracket segment (Max Principal: 3.2 MPa), (e) M24–M40 segment (Max Principal: 0.29 MPa), and (f) M41 segment (Max Principal: 2.92 MPa)

According to the analysis results, the main body of the tower cylinder meets the crack resistance requirements, and only very small local stress concentrations exist. These affect only a few very small mesh elements and are attributed to local mesh distortion or to the pre-stress anchorage ends. If these elements are disregarded, the whole concrete tower cylinder meets the crack resistance requirements.

5.4 Decompression checking calculation under S_3 working condition

According to IEC 61400-6 (2020) specification, the concrete shall be checked for decompression at the S_3 level, i.e. to ensure that the whole concrete section remains in compression under the S_3 loads, gravity, and pre-stress. Figure 8 shows the S_{33} stress contour plot of concrete tower cylinder under S_3 level. S_{33} is the stress component in the vertical direction. The part with negative S_{33} stress is the compression area, and the part with positive S_{33} stress is the tensile area. The tensile areas are shown in white.

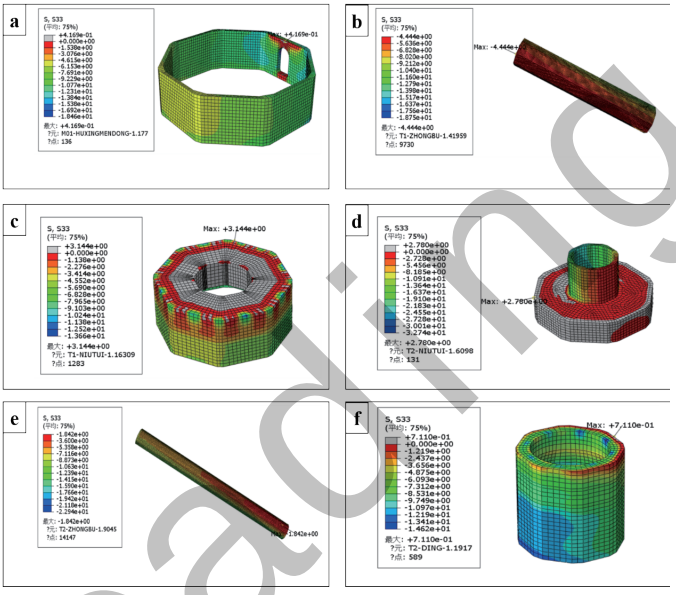


Figure 8. Stress contour plot of concrete tower cylinder S_{33}: (a) M01 door opening segment (Max S_{33}: 0.41 MPa), (b) M02–M21 segment (Max S_{33}: -4.44 MPa), (c) M22 bracket segment (Max S_{33}: 3.14 MPa), (d) M23 bracket segment (Max S_{33}: 2.78 MPa), (e) M24–M40 segment (Max S_{33}: -1.84 MPa), and (f) M41 segment (Max S_{33}: 0.71 MPa)

According to the analysis results, tensile stress occurs only at the pre-stressed ends of the bracket segments of the concrete tower cylinder, with very small tensile stresses at the M01 door opening and in M41. If the local stress concentration is ignored, the tower cylinder satisfies the full-section compression requirement. Therefore, in the vertical direction, there is no obvious tensile stress in the concrete tower body, which satisfies the principle of full-section compression.

6. Finite element analysis results of the externally pre-stressed tower cylinder (EP-C_{80})

In recent years, externally pre-stressed structures have developed rapidly. Compared with the internally pre-stressed tower cylinder, the externally pre-stressed (unbonded) tower cylinder has several advantages (Ariyawardena and Ghali, 2002). First, duct forming and grouting are avoided, which greatly reduces the friction loss of pre-stress, and a variety of tendon profiles can be selected according to actual needs (Zhu et al., 2015). Second, since no pre-stressing ducts need to be reserved, the wall thickness of the tower cylinder can be reduced appropriately, which reduces the weight and cost of the tower cylinder and simplifies construction because grouting and similar operations are unnecessary (Kaur and

Proof Reading

Singh, 2017). Third, in terms of mechanical performance, the bearing capacity of an externally pre-stressed structure is not reduced by reserved holes (Virlogeux, 1990).

Under the serviceability limit state, there is still a certain compressive stress reserve at the most unfavorable position of the structure. Because the section is not weakened by reserved holes, the bending capacity of the structure is improved to a certain extent (Li, 2008; Gong, 2012). However, the externally pre-stressed tower cylinder also has some disadvantages, such as corrosion of the pre-stressed tendons and the secondary effect caused by external pre-stressing (Wu et al., 2025). Because the tendons are separated from the concrete except at the anchorage ends and deviator blocks, they cannot deform compatibly with the tower cylinder. The larger the deformation of the tower cylinder, the larger the relative offset between the tendons and the tower cylinder, which reduces the effective lever arm of the tendons and thereby reduces the bearing capacity of the structure. The secondary effect is therefore unfavorable to the structure, and its impact should be reduced. It can be reduced by providing deviator blocks at a suitable spacing (Zeng et al., 2019).

In this study, the internal pre-stressing tendons of the typical tower cylinder were replaced with external pre-stressing tendons, and the relevant mechanical properties of the tower cylinder under the two pre-stressing systems were compared to provide a reference for the optimal design of the structure. In the finite element model, the difference from the internally pre-stressed tower cylinder is that the externally pre-stressed tower cylinder requires a deviator block in the middle of each plate. Because the tendons are unbonded, tie constraints are used between the tendons and the deviator blocks instead of embedded constraints, as shown in Figure 9. All other settings are the same as for the internally pre-stressed tower cylinder.

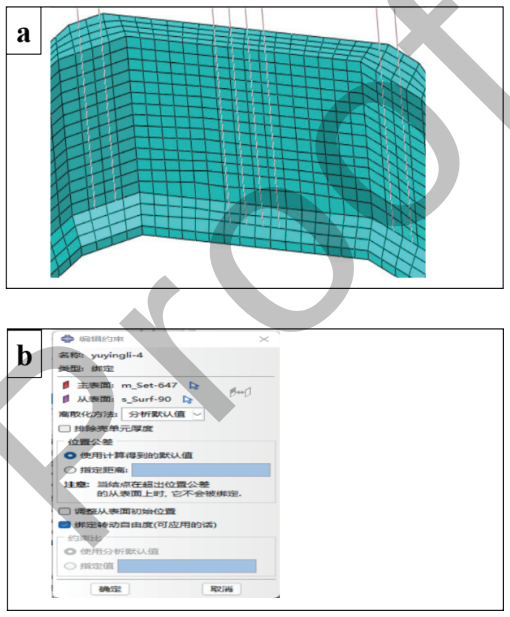


Figure 9. Modeling of external pre-stressed tower cylinder: (a) modeling of external pre-stressed tendons and (b) constraint setting of external pre-stress

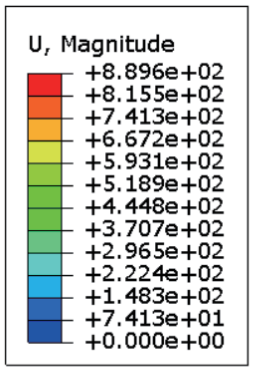




Figure 10. Contour plot of tower displacement

6.1Checking calculation of tower top lateral displacement under S1 working condition

Under S_1 working condition, the maximum horizontal displacement of the wind turbine tower top is 889.6 mm, which is less than the allowable displacement of 1975 mm (L/100). The displacement of the wind turbine tower cylinder under load meets the specification requirements, as shown in Figure 10.

6.2 Checking calculation of principal compressive stress under S_1 working condition

1.Stress checking calculation of concrete tower cylinder

According to IEC 61400-6 (2020) specification, the maximum compressive stress limit of C_{80} concrete is 38.4 MPa at S_1 level. Except for the M22 and M23 corbel segments, all other concrete segments meet the requirements of the specification (Figure 11). Because of the variable cross-section of the M22 and M23 corbel segments and the anchorage ends of the external pre-stressed tendons, stress concentration occurs at the abrupt section changes and at the pre-stress anchorage ends, where the principal compressive stress is greater than the limit value required by the specification.

2.Checking calculation of reinforcement stress

According to IEC 61400-6 (2020), under S_1 level, the tensile stress in ordinary reinforcement shall not exceed 360 MPa, and the stress of pre-stressed reinforcement (after short-term loss) shall not exceed 1395 MPa. Even with the local stress concentrations included, the stresses in the ordinary and pre-stressed reinforcement of the structure meet the requirements (Figure 12).

Proof Reading

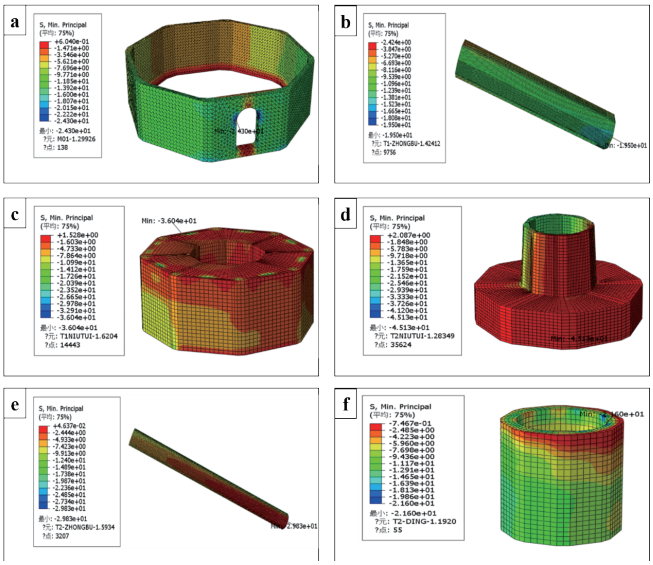


Figure 11. Contour plot of principal compressive stress of concrete tower cylinder: (a) M01 door opening segment (Min Principal: 24.30 MPa), (b) M02–M21 segment (Min Principal: 19.50 MPa), (c) M22 bracket segment (Min Principal: 36.04 MPa), (d) M23 bracket segment (Min Principal: 45.13 MPa), (e) M24–M40 segment (Min Principal: 29.83 MPa), and (f) M41 segment (Min Principal: 21.60 MPa)

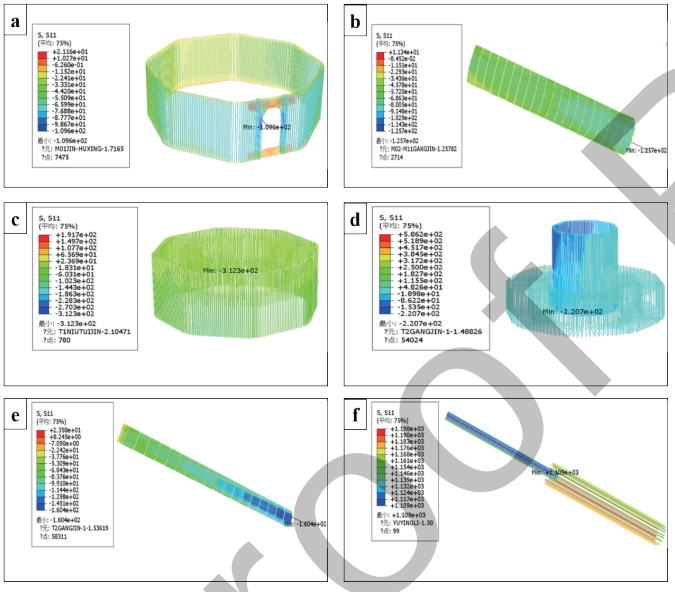


Figure 12. Stress contour plot of concrete tower cylinder reinforcement: (a) M01 door opening segmental reinforcement (S11 Max: 109.60 MPa), (b) M02–M21 segment reinforcement (S11 Max: 125.70 MPa), (c) M22 bracket segment reinforcement (S11 Max: 312.30 MPa), (d) M23 bracket segment reinforcement (S11 Max: 220.70 MPa), (e) M24–M41 segment reinforcement (S11 Max: 160.40 MPa), and (f) Pre-stressed reinforcement (S11 Max: 1109.00 MPa)

6.3 S_2 checking calculation of crack resistance under working conditions

Figure 13 shows the principal tensile stress contour plot of externally pre-stressed concrete tower cylinder at S_2 level.

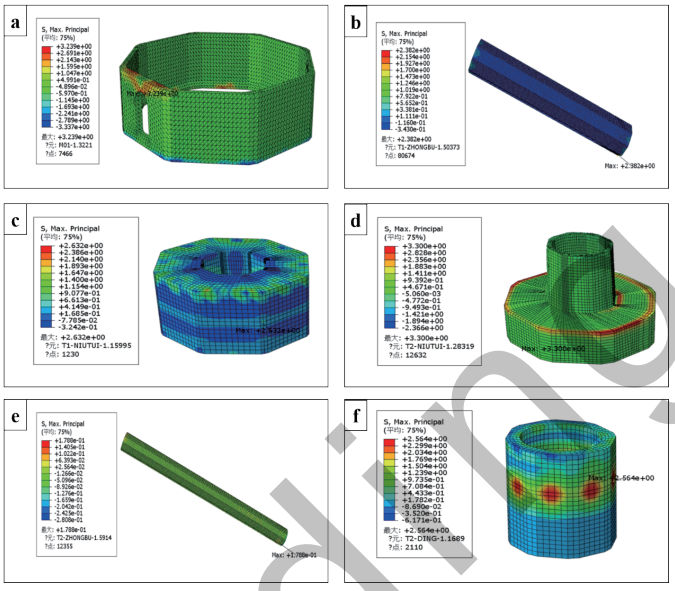


Figure 13. Contour plot of principal tensile stress of concrete tower cylinder: (a) M01 door opening segment (Max Principal: 3.24 MPa), (b) M02–M21 segment (Max Principal: 2.38 MPa), (c) M22 bracket segment (Max Principal: 2.63 MPa), (d) M23 bracket segment (Max Principal: 3.30 MPa), (e) M24–M40 segment (Max Principal: 0.18 MPa), and (f) M41 segment (Max Principal: 2.56 MPa)

According to the analysis results, the main body of the tower cylinder meets the crack resistance requirements, and only very small local stress concentrations exist. These affect only a few very small mesh elements and are attributed to local mesh distortion or to the pre-stress anchorage ends. If these elements are disregarded, the whole concrete tower cylinder meets the crack resistance requirements.

6.4 Pressure relief checking calculation under S_3 working condition

Figure 14 shows the S_{33} stress contour plot of concrete tower cylinder under S_3 level. S_{33} is the stress component in the vertical direction. The part with negative S_{33} stress is the compression area, and the part with positive S_{33} stress is the tensile area. The tensile areas are shown in white.

According to the analysis results, tensile stress occurs only at the pre-stressed ends of the bracket segments of the concrete tower cylinder, with very small tensile stresses at the M01 door opening and in M41. If the local stress concentration is ignored, the tower cylinder satisfies the full-section compression requirement.

7.Comparison of finite element calculation results

7.1 Comparison of tower top displacement under S_1 working condition

Proof Reading

Figure 15 shows that the lateral displacement curves of the internally and externally pre-stressed tower cylinders are almost coincident. Therefore, the arrangement of internal and external pre-stressed tendons has little effect on the lateral displacement of the tower cylinder. Figure 16a shows the relationship curve between the base shear force and the tower top displacement. The base shear force is the horizontal shear force at the bottom of the tower (Huang et al., 2022). Both curves are approximately linear, indicating that the tower cylinder is in the elastic stage. Figure 16b shows the relationship curve between the base shear force and the displacement level. The displacement level is the ratio of the displacement to the displacement limit (1975 mm). The displacement level should not be greater than 1/100. It can be seen from the figure that the maximum displacement levels are less than 1/100, which meets the requirements.

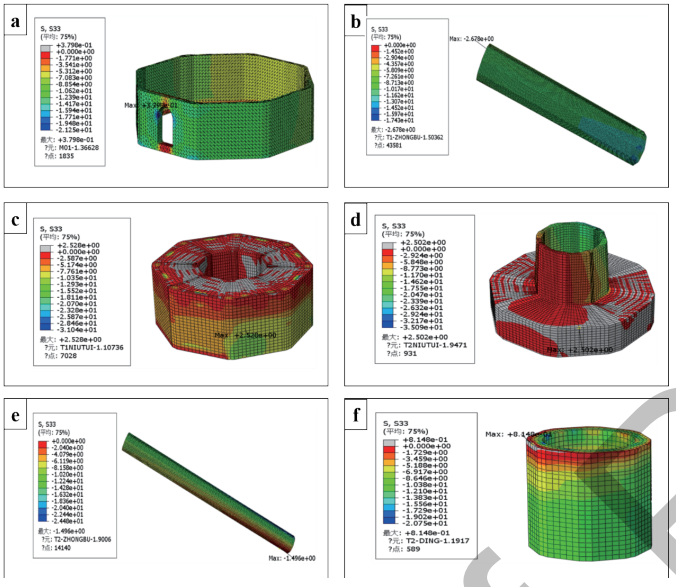


Figure 14. Stress contour plot of concrete tower cylinder S_{33}: (a) M01 door opening segment (Max S_{33}: 0.38 MPa), (b) M02–M21 segment (Max S_{33}: -2.68 MPa), (c) M22 bracket segment (Max S_{33}: 2.53 MPa), (d) M23 bracket segment1 (Max S_{33}: 2.50 MPa), (e) M24–M40 segment (Max S_{33}: -1.50 MPa), and (f) M41 segment (Max S_{33}: 0.81 MPa)

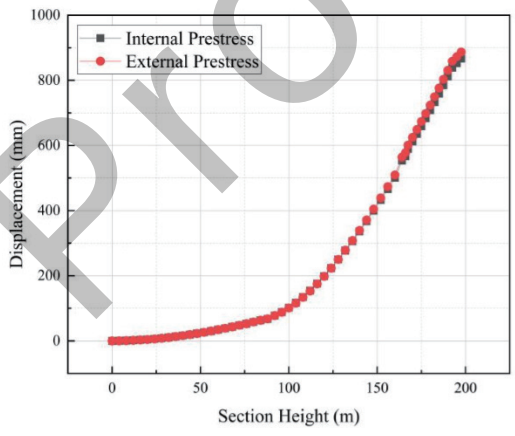


Figure 15. Comparison of tower cylinder top displacement of internal and external pre-stressed tower cylinder

The negligible difference observed between the internal and external pre-stressed tower cylinders in horizontal lateral displacement agrees with previous numerical and experimental studies on hybrid and pre-stressed wind-turbine towers, which found that tendon layout has only a minor influence on global lateral stiffness compared to overall geometry and composite section rigidity (Tomczak, 2021; Huang et al., 2022). Similar analyses showed that both internal and external post-tensioning primarily modify axial stress states while the lateral displacement under service loading remains nearly unchanged (Lotfy, 2012). The linear relationship between base shear and tower-top displacement obtained here is also consistent with results from finite-element simulations of pre-stressed concrete towers, which remain elastic up to service-level wind loading (Chen et al., 2020). Moreover, the maximum displacement ratio below 1/100 satisfies the IEC 61400-6 (2020) serviceability criterion, confirming that the present tower design maintains sufficient stiffness under S_1 loading.

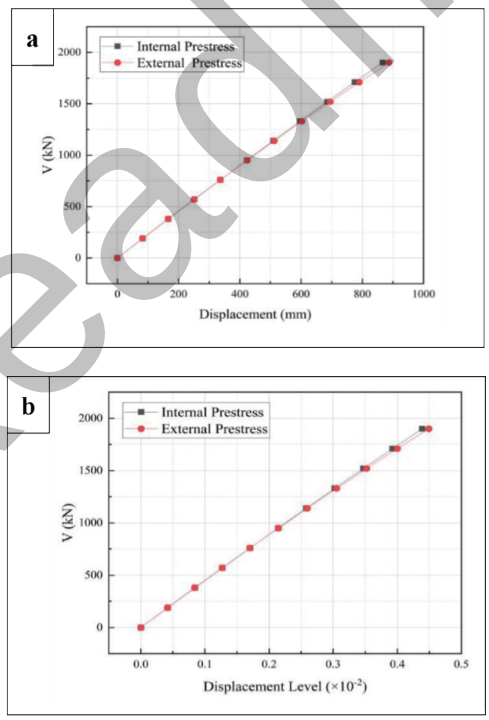


Figure 16. (a) Base shear force versus tower-top displacement and (b) base shear force versus displacement level

7.2 Comparison of results under S_1 working condition

The base shear–strain curve was extracted at the critical point (i.e., the location of maximum stress) of each segment of the internally and externally pre-stressed tower cylinders. The strain is represented as logarithmic (true) strain, corresponding to the parameter LE in ABAQUS. Logarithmic strain reflects the cumulative process of deformation, since it is the sum of the strain increments provided that the direction of the principal strain axes remains unchanged.

Figure 17 shows that the critical points of most segments remain within the elastic range, while local stress concentration

Proof Reading

occurs at the corbel segment near the anchorage ends of the pre-stressed tendons. If this local stress concentration is disregarded, the overall compression behavior of the tower cylinder can be considered to remain elastic. Under the same base shear force, the principal compressive strain of the externally pre-stressed tower cylinder is greater than that of the internally pre-stressed tower cylinder.

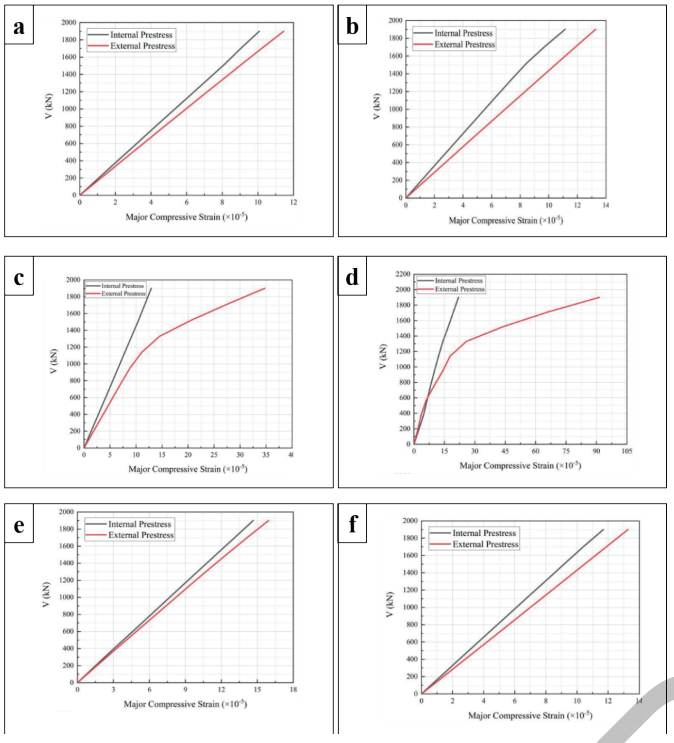


Figure 17. Base shear strain curve at critical points of each segment: (a) M01 door opening segment, (b) M02–M21 segment, (c) M22 bracket segment, (d) M23 bracket segment, (e) M24–M40 segment, and (f) M41 segment

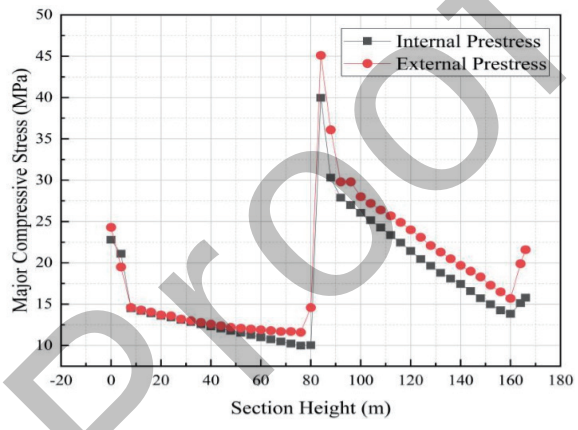


Figure 18. Comparison of principal compressive stress of internal and external pre-stressed tower cylinder along the tower body

Figure 18 shows that the principal compressive stress of the externally pre-stressed tower cylinder along the section height is slightly greater than that of the internally pre-stressed tower cylinder, which is considered to be mainly caused by the secondary effect of the external pre-stressed tendons. The variation of the principal compressive stress along the section height is consistent for the two cylinders, and local stress concentration occurs in the bottom M01 door opening segment, the middle bracket segment, and the top transition section; the stress concentration is more pronounced in the externally pre-stressed tower cylinder.

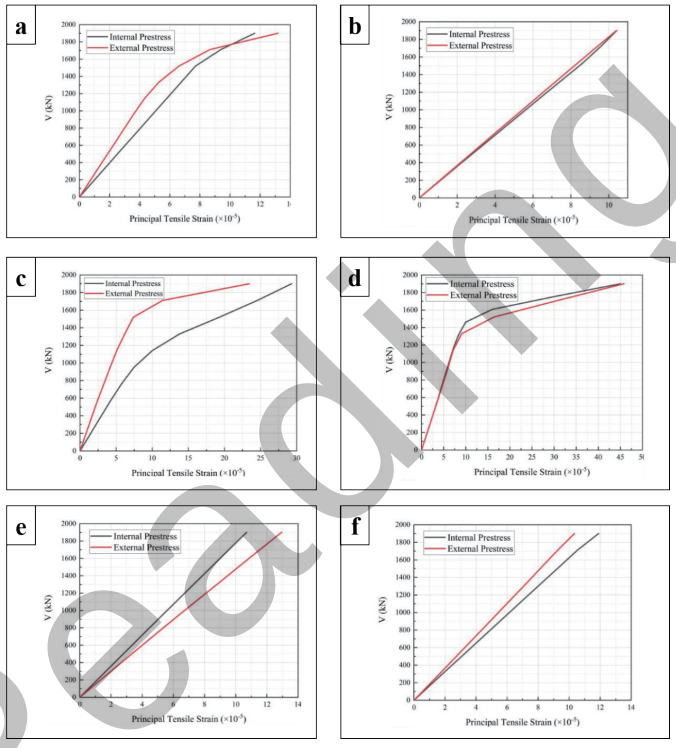


Figure 19. Base shear strain curve at critical points of each segment: (a) M01 door opening segment, (b) M02–M21 segment, (c) M22 bracket segment, (d) M23 bracket segment, (e) M24–M40 segment, and (f) M41 segment

The stress concentration in the M01 door opening segment is mainly caused by the weakening of the segment by the door opening. The stress concentration in the middle bracket segment mainly occurs at the anchorage ends of the pre-stressed tendons. Because the finite element model is simplified and the anchorage is not modeled, the stress concentration here may be overestimated; in the actual structure, the anchorage, together with a steel plate at the tendon end, will reduce it. The top transition section is connected to the steel tower section, and its top is also the anchorage end of the pre-stressed tendons; local stress concentration therefore also occurs there.

The finding that most tower segments remained within the elastic range, with only local stress concentration at the corbel anchorage zones, is consistent with earlier finite element studies of pre-stressed wind-turbine towers, which reported elastic behavior over the majority of the height under service wind loads and localized yielding near tendon anchorages or geometric discontinuities (Tomczak, 2021). The slightly higher principal compressive strain and stress in the externally pre-stressed configuration correspond with observations that

Proof Reading

external tendons introduce secondary bending effects due to their eccentricity and reduced composite restraint (Lotfy, 2012; Huang et al., 2022). Similar local stress concentrations at door openings, bracket supports, and tendon anchorages were also noted in experimental and numerical analyses of pre-stressed concrete towers and pylons, where strengthening plates or localized reinforcement were recommended to reduce peak stress values (Chen et al., 2020). These agreements suggest that the modeled stress distribution and concentration zones are plausible, and the overall elastic response indicates adequate stiffness under the serviceability loads considered.

7.3 Comparison of results under S2 working condition

Figure 19 shows that local stress concentration occurs in the M01 door-opening segment near the entrance and in the corbel segment near the anchorage ends of the pre-stressed tendons, while the other segments remain within the elastic range. Structural measures can be taken to reduce the stress in these local zones. If the local stress concentration is disregarded, the overall tensile behavior of the tower cylinder can be considered to remain elastic. On the whole, under the same base shear force, the principal tensile strain of the externally pre-stressed tower cylinder is smaller than that of the internally pre-stressed tower cylinder.

Figure 20 shows that the principal tensile stress of the externally pre-stressed tower cylinder along the section height is slightly smaller than that of the internally pre-stressed tower cylinder. The variation of the principal tensile stress along the section height is the same for the two cylinders, with local stress concentrations in the M01 door opening segment at the bottom, the bracket segments at mid-height, and the transition section at the top. Enlarged views of the local zones are shown in Figure 21.

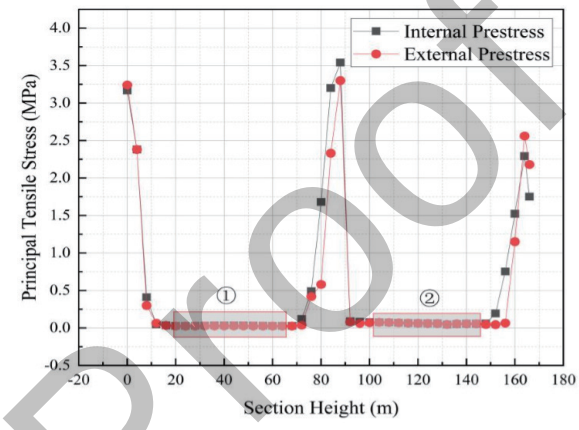


Figure 20. Comparison of principal tensile stress of internal and external pre-stressed tower cylinders along the tower body

7.4 Comparison of vertical stress results under S_3 working condition

Figure 22 shows that, for both the internally and externally pre-stressed tower cylinders, the maximum vertical stress exceeds zero only locally; that is, the M01 door opening segment, the bracket segments, and the M41 segment have local tensile areas, which are mainly caused by stress concentration at the pre-stress anchorage ends. Structural measures can be taken to reduce the stress concentration at these ends. Except for the local stress concentrations, the rest of the tower cylinder satisfies the full-section compression requirement. On the whole, the maximum vertical stress of the externally pre-stressed tower cylinder along the height is slightly smaller than that of the internally pre-stressed tower cylinder.

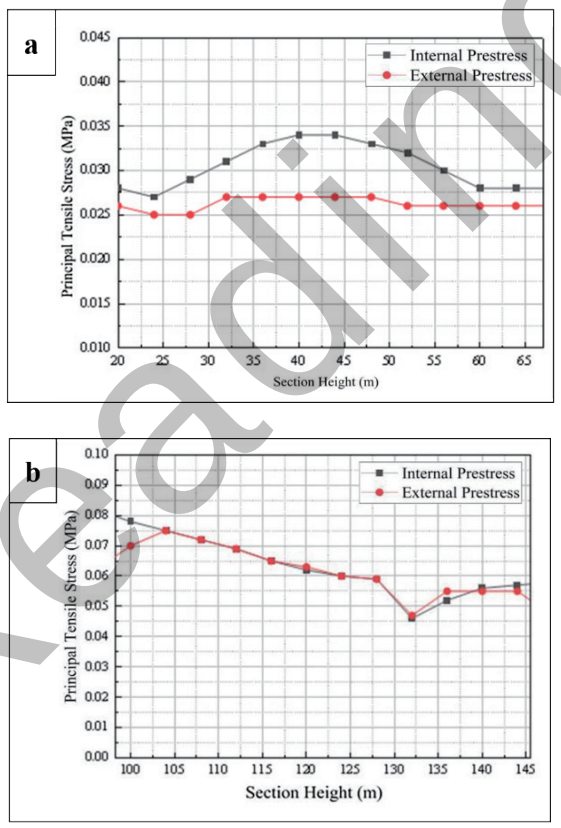


Figure 21. Comparison of principal tensile stress of internal and external pre-stressed tower cylinder along the tower body: (a) partial enlarged drawing ① and (b) partial enlarged drawing ②

The occurrence of localized tensile stress at the door opening, bracket, and top segments corresponds well with observations from previous analyses of pre-stressed concrete and hybrid wind-turbine towers. Studies have shown that anchorage zones and geometric discontinuities commonly develop localized tensile stresses due to pre-stress transfer and secondary bending effects, which can be effectively mitigated through proper end-zone reinforcement or anchorage plate detailing (Mao et al., 2018). Numerical investigations on ultra-high-performance concrete (UHPC) hybrid wind-turbine towers similarly reported that while the tower body largely remained under full-section compression, small tensile regions appeared near transition and connection zones under combined wind and gravity loads (Wu et al., 2022). Furthermore, finite-element analysis of pre-stressed concrete wind-turbine towers with circular cross-sections confirmed

Proof Reading

that the overall stress distribution remains predominantly compressive along the height, and any local tensile zones occur only at anchorage ends or openings (de Lana et al., 2021). The slightly lower maximum vertical stress observed in the externally pre-stressed configuration aligns with the tendency of external tendons to induce more favorable compression distribution along the tower wall owing to their eccentricity, thereby reducing peak compressive stresses near the inner surface.

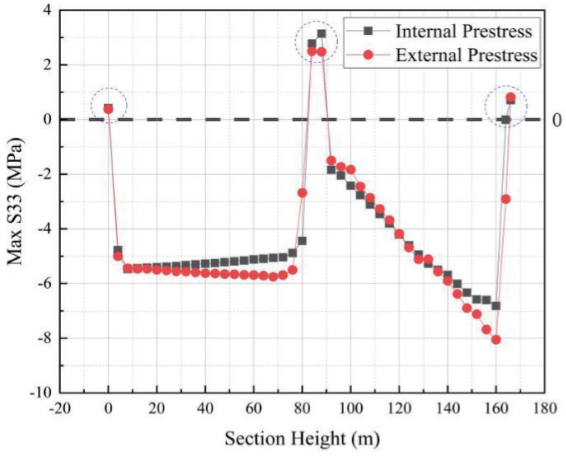


Figure 22. Comparison of maximum vertical stress of internal and external pre-stressed tower cylinder along the tower body

8. Conclusion

This paper presented the conceptual design of a 200 m pre-stressed self-lifting steel–concrete composite tower. The specific design parameters of the structure, the connections between the tower segments, and the advantages of the tower were described first. A finite element model of the tower was then established in ABAQUS, and its element types, contact settings, boundary conditions, load application, and constitutive relationships were introduced. For the load application, particular attention was paid to the treatment of the pre-stressed tendons: the cooling method was used to apply the pre-stress, the pre-stress losses were calculated to obtain the effective pre-stress, and the cooling temperature of each tendon segment was then calculated from the relevant formulas. Finally, static analyses were carried out according to the relevant specifications, and the lateral displacement and stress of the tower under the S_1 working condition, the crack resistance under the S_2 working condition, and the decompression of the section under the S_3 working condition were checked.

The results show that the tower cylinder has good mechanical performance. The stresses in the internally and externally pre-stressed tower cylinders were also compared. For the tower geometry and tendon configuration considered in this study, the arrangement of internal or external pre-stressed tendons has little effect on the horizontal displacement of the tower cylinder. The influence of tendon eccentricity, pre-stress level, and deviator spacing requires further parametric study. Under the S_1 condition, the principal compressive stress of the externally pre-stressed tower cylinder along the section height is slightly greater than that of the internally pre-stressed tower cylinder. Under the S_2 working condition, the principal tensile stress of the externally pre-stressed tower cylinder along the section height is slightly smaller than that of the internally pre-stressed tower cylinder. Under the S_3 working condition, the maximum vertical stress along the height of the externally pre-stressed tower cylinder is slightly smaller than that of the internally pre-stressed tower cylinder. Except for small local tensile stresses, the rest of the tower cylinder meets the full-section compression requirement.

Acknowledgments

The research described in this paper was financially supported by the National Natural Science Foundation of China (Grant No. 52178195) and the project “Key Technology Research on Ultra High Performance Concrete (UHPC) Wind Power Hybrid Tower System” (Project No. SA10000003512023054).

Declaration of Interest Statement

The authors declare that they have no known competing financial interests or personal relationships that could have influenced the work reported in this study.

References

[1] Ariyawardena, N., & Ghali, A. (2002). Pre-stressing with unbonded internal or external tendons: Analysis and computer model. Journal of Structural Engineering, 128(12), 1493–1501.

[2] Barbero, E. J. (2023). Finite element analysis of composite materials using Abaqus®. CRC Press.

[3] Bazeos, N., & Hatzigeorgiou, G. D. (2002). Static, seismic, and stability analyses of a prototype wind turbine steel tower. Engineering Structures, 24, 1015–1025.

[4] Brughuis, F. J. (2003). Advanced tower solutions for large wind turbines and extreme tower heights. In Proceedings of the 2003 European Wind Energy Conference and Exhibition (pp. 16–19). European Wind Energy Association.

[5] Chen, J., et al. (2020). Numerical investigation of strengthening by circumferential pre-stressing to improve fatigue life of embedded-ring concrete foundation for onshore wind turbine tower. Energies, 13(3), 533.

[6] de Lana, J. A., et al. (2021). Behavior study of pre-stressed concrete wind-turbine tower in circular cross-section. Engineering Structures, 227, Article 111406.

[7] Dong, C. (2015). Research on mechanical properties of steel–concrete composite structure wind power tower [Doctoral dissertation, Harbin Institute of Technology].

[8] Gong, H. (2012). Application potential of externally pre-stressed structures. In Proceedings of the Academic Exchange on Building Technology and Management (pp. 180, 182) [Publisher unknown].

[9] Gu, F. (2009). Research on steel–concrete composite tower for wind turbine [Doctoral dissertation, Xinjiang Agricultural University].

[10] Gudayu, A. D., Steuernagel, L., & Meiners, D. (2022). The capability of ABAQUS/CAE to predict the tensile properties of

Proof Reading

sisal fiber reinforced polyethylene terephthalate composites. Composites and Advanced Materials, 31, 26349833221137602.
[11] Huang, X., Li, B., Zhou, X., Wang, Y., & Zhu, R. (2022, January). Geometric optimisation analysis of steel–concrete hybrid wind turbine towers. In Structures (Vol. 35, pp. 1125–1137). Elsevier.
[12] International Electrotechnical Commission. (2020). IEC 61400-6: Wind energy generation systems – Part 6: Tower and foundation design requirements [Standard]. Geneva, Switzerland.
[13] Kaur, H., & Singh, J. (2017). A review on external pre-stressing in concrete. International Research Journal of Engineering and Technology, 4, 1801–1805.
[14] Li, M. (2008). Stress analysis and application of externally pre-stressed concrete structure. Transportation World (Construction and Maintenance, Machinery), 2008(05), 142–143.
[15] Liu, Y. (2016). Research on key technology of steel–concrete composite structure wind power tower design [Doctoral dissertation, Harbin Institute of Technology].
[16] Lotfy, I. (2012). Pre-stressed-concrete-wind-turbine-supporting-system. Precast/Pre-stressed Concrete Institute.
[17] Ma, X., Zeng, S., & Dong, C. (2014). Design of assembled post-tensioned pre-stressed reactive powder concrete wind turbine tower. Advanced Materials Research, 28(11), 38–43.
[18] Mao, W., Gou, H., He, Y., & Pu, Q. (2018). Local stress behavior of post-tensioned prestressed anchorage zones in continuous rigid frame arch railway bridge. Applied Sciences, 8(10), 1833.
[19] Ministry of Housing and Urban–Rural Development of the People's Republic of China. (2010). GB 50010-2010: Code for design of concrete structures [Standard]. China Construction Industry Press.
[20] Ministry of Housing and Urban–Rural Development of the People's Republic of China. (2019). GB 50135-2019: Design standard for high-rise structures [Standard]. China Planning Press.
[21] Shan, L. (2009). Research on structure selection and mechanical performance of wind turbine tower [Doctoral dissertation, Harbin Institute of Technology].
[22] Shi, R., & Zhang, J. (2021). Research on optimization technology of building seismic design based on Abaqus. Modern Electronic Technology, 44(18), 119–122.
[23] Song, Y., & Chen, Y. (2012). Design and analysis of a separate pre-stressed concrete tower for wind power generation. Special Structure, 29(4), 47–49.
[24] Tomczak, J. (2021). Finite element analysis of post-tensioned concrete wind turbine towers (Master's thesis). University of Minnesota.
[25] Vernardos, S. M., et al. (2021). Experimental and numerical investigation of steel–grout–steel sandwich shells for wind turbine towers. Journal of Constructional Steel Research, 184, 106815.
[26] Virlogeux, M. P. (1990). External pre-stressing: From construction history to modern technique and technology. ACI SP-120: External Pre-stressing in Bridges, 1–60.
[27] Wang, C., Li, H., Hu, S., Xu, D., & Wang, J. (2019). Numerical model and calculation analysis of pre-stressed steel–concrete ultra-high wind power tower. Building Structure, 49(S_1), 955–958.
[28] Wu, X., Zhang, X., Bhattarai, H. B., Hwang, H. J., Yang, J., & Kang, S. (2022). Structural behavior analysis of UHPC hybrid tower for 3-MW super tall wind turbine under rated wind load. International Journal of Concrete Structures and Materials, 16(1), 52.
[29] Wu, Y., Chen, B., Lopes, S. M., Lopes, A. V., & Lou, T. (2025, January). A critical review of pre-stressed concrete structures with external FRP tendons. In Structures (Vol. 71, p. 108049). Elsevier.
[30] Xin, Y. (2015). Analysis of the relationship between compressive strength of concrete cylinder specimens and cube specimens. Hydropower and Electrification in China, 2015(07), 59–62.
[31] Zeng, B., Shang, R., & Xu, Q. (2019). Secondary effect analysis of externally pre-stressed reinforced structures. Industrial Buildings, 49(12), 96–99, 104.
[32] Zhang, D. (2015). Model test and analysis of pre-stressed concrete wind turbine tower [Doctoral dissertation, Shanghai Jiao Tong University].
[33] Zhou, S., Wang, J., & Leng, F. (2015). Pre-stress simulation methods and comparison in finite element calculation of concrete structures. People's Yangtze River, 46(24), 38–42, 47.
[34] Zhu, H., Yang, Y., & Fan, W. (2015). External pre-stressing bridge reinforcement technology review. In MATEC Web of Conferences (Vol. 22, p. 04028). EDP Sciences.

Proof Reading